# Morphological Control of Room-Temperature Ionic Liquid Templated Mesoporous Silica Nanoparticles for Controlled Release of Antibacterial Agents

**ARTICLE** *in* NANO LETTERS · SEPTEMBER 2004

Impact Factor: 13.59 · DOI: 10.1021/nl048774r



**3 AUTHORS**, INCLUDING:

Brian G Trewyn
Colorado School of Mines
**63** PUBLICATIONS **6,969** CITATIONS
SEE PROFILE

Chad Whitman
Bio-Rad Laboratories
**4** PUBLICATIONS **288** CITATIONS
SEE PROFILE

NANO LETTERS

2004
Vol. 4, No. 11
2139−2143

# Morphological Control of Room-Temperature Ionic Liquid Templated Mesoporous Silica Nanoparticles for Controlled Release of Antibacterial Agents

**Brian G. Trewyn, Chad M. Whitman, and Victor S.-Y. Lin***

*Department of Chemistry, Iowa State University, Ames, Iowa 50011-3111*

*Received July 29, 2004; Revised Manuscript Received September 12, 2004*

**ABSTRACT**

**A series of room-temperature ionic liquid (RTIL) containing mesoporous silica nanoparticle (MSN) materials with various particle morphologies, including spheres, ellipsoids, rods, and tubes, were synthesized. By changing the RTIL template, the pore morphology was tuned from the MCM-41 type of hexagonal mesopores to rotational moiré type of helical channels, and to wormhole-like porous structures. These materials were used as controlled release delivery nanodevices to release antibacterial ionic liquids against *Escherichia coli K12*.**

Structurally well-defined mesoporous silica materials, such as MCM-41/48,[1] SBA-15,[2] MSU-n,[3] KIT-1,[4] and FSM-16,[5] have recently attracted much attention for their potential applications in sensing,[6] catalysis,[7] and drug delivery.[8] These materials are typically synthesized by utilizing organic surfactants or block copolymers as structure-directing templates in acid- or base-catalyzed condensation of alkoxysilanes. Obviously, the realization of the aforementioned applications for mesoporous silica materials greatly depends on the ability of controlling not only the intraparticle, but also the interparticle mass-transport processes. Therefore, it is important to develop methods to regulate both the pore and particle morphology of these materials.[9]

To this goal, several recent reports[10] have focused on the utilization of other amphiphilic molecules, such as room-temperature ionic liquids (RTILs), as templates for the synthesis of mesoporous silica materials. For example, Zhou et al.[10a−c] have demonstrated that monolithic mesoporous silicas with either wormlike pores or lamellar supermicroporous structures could be prepared by using 1-alkyl-3-methylimidazolium ($C_n$MIM, $n$ = the number of carbons in the alkyl chain) chloride or tetrafluoroborate, respectively, as templates. Also, Dai and co-workers[10d] have successfully synthesized periodic mesoporous organosilica (PMO) materials by using two different $C_n$MIM bromide templates in the condensation reaction of bis(triethoxysilyl)ethane. Despite these recent advancements, no study has been reported on how the particle morphology (size and shape) could be regulated by these RTILs. Herein, we report on the synthesis and characterization of a series of mesoporous silica nanoparticle (MSN) materials with various porous structures and particle shapes, such as spheres, ellipsoids, rods, and tubes, by using different RTIL templates, such as 1-tetradecyl-3-methylimidazolium bromide ($C_{14}$MIMBr), 1-hexadecyl-3-methylimidazolium bromide ($C_{16}$MIMBr), 1-octadecyl-3-methylimidazolium bromide ($C_{18}$MIMBr), and 1-tetradecyloxymethyl-3-methylimidazolium chloride ($C_{14}$OCMIMCl), respectively (Figure 1). To study the mass-transport properties of the $C_n$MIM-MSN materials, we investigated the controlled release profiles of these materials by utilizing the RTIL templates as antibacterial agents against the Gram (−) microbe *Escherichia coli K12* as depicted in Figure 2. Our results indicated that the rates of RTIL release from the MSN materials are governed by the particle and pore morphology leading to different antibacterial activities.

First, we synthesized the $C_{14}$MIMBr, $C_{16}$MIMBr, and $C_{18}$MIMBr RTILs by reacting 1-methylimidazole (50 mmol) with 50 mmol of 1-bromotetradecane, 1-bromohexadecane, and 1-bromooctadecane, respectively, at 90 °C for 48 h. The products were purified by recrystallization in THF. The resulting white crystals were collected by filtration and dried under vacuum at room temperature. The $C_{14}$OCMIMCl was prepared via a literature procedure.[11] In a typical procedure for the synthesis of the $C_n$MIM-MSN materials, a selected $C_n$MIM RTIL (2.74 mmol) was first dissolved in 480 mL of 15 mM NaOH(aq). The solution was heated to 80 °C, followed by a dropwise addition of tetraethyl orthosilicate

* Corresponding author. Phone: (515) 294-3135. E-mail: vsylin@iastate.edu.

10.1021/nl048774r CCC: $27.50 
**Published on Web 09/28/2004**

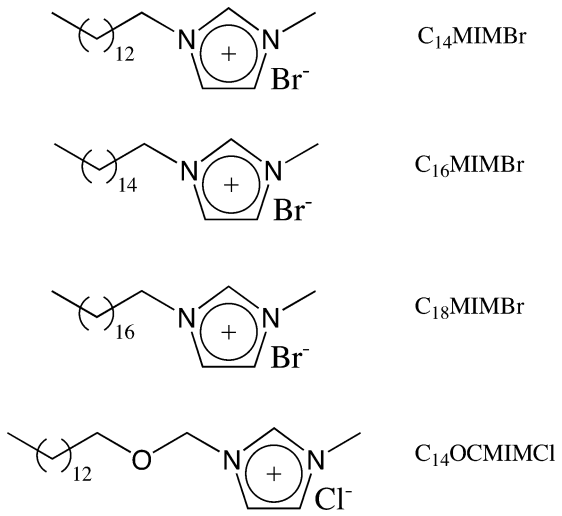


**Figure 1.** Chemical structures of 1-tetradecyl-3-methylimidazolium bromide ($C_{14}$MIMBr), 1-hexadecyl-3-methylimidazolium bromide ($C_{16}$MIMBr), 1-octadecyl-3-methylimidazolium bromide ($C_{18}$MIMBr), and 1-tetradecyloxymethyl-3-methylimidazolium chloride ($C_{14}$OCMIMCl).

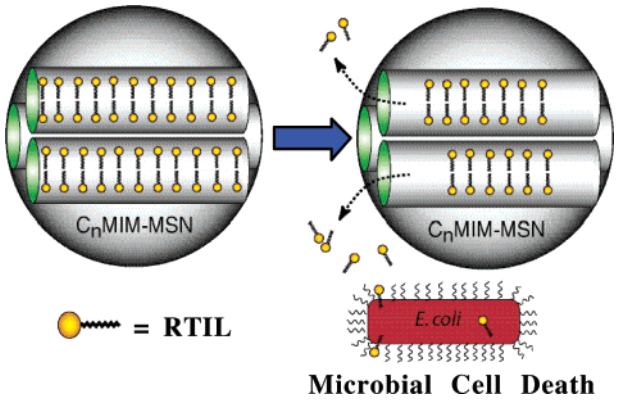


**Figure 2.** Schematic representation of the controlled release process of $C_n$MIM-MSN and its antibacterial activity against *E. coli*.

(22.4 mmol) and stirred for 2 h to yield the desired $C_n$MIM-MSN material.

To characterize the mesoporous structures of the $C_n$MIM-MSN materials, the $C_n$MIM RTILs were extracted from the mesopores by refluxing the as-synthesized $C_n$MIM-MSN (500 mg) in 200 mL of methanolic solution of HCl (520 mM) for 48 h. As revealed by the transmission electron micrographs (TEM) in Figure 3, $C_n$MIM-MSNs synthesized with the four different RTIL templates exhibited different particle morphologies. For example, the $C_{14}$MIM-MSN material showed spherical particles with diameters ranging from 100 to 300 nm, as depicted in Figure 3a. Interestingly, upon replacing the $C_{14}$MIMBr with other structurally similar RTILs with longer alkyl chains, such as $C_{16}$MIMBr and $C_{18}$MIMBr (Figure 3b,c), the shapes of the MSN materials transformed into ellipsoids and rods, respectively. Furthermore, substituting the $C_{16}$MIM template with a similar sized $C_{14}$OCMIM RTIL gave rise to the $C_{14}$OCMIM-MSN material (Figure 3d) consisting of tubular shaped particles.

The pore morphologies of the $C_n$MIM-templated MSNs were determined by nitrogen adsorption−desorption surface analysis (BET isotherms and BJH pore size distributions), TEM (Figure 3), and powder X-ray diffraction (XRD) spectroscopy (Figure 4). All four $C_n$MIM-MSN materials exhibited type IV BET isotherms. Also, the BJH average pore diameters of these materials increased as the organic regions of the RTILs lengthened (Table 1). Hexagonally packed mesoporous channels were clearly observed in the TEM micrographs of the $C_{14}$MIM- and $C_{16}$MIM-MSNs (Figure 3a,b). In addition, both materials exhibited diffraction patterns characteristic of hexagonal MCM-41 silicas, including (100), (110), (200), and (210) peaks as depicted in Figure 4a,b.

**Table 1.** Nitrogen Sorption Data of $C_n$MIM-MSN Material

| | BET surface area ($m^2$/g) | pore volume ($cm^3$/g) | BJH average pore diameter (Å) |
|---|---|---|---|
| $C_{14}$MIM-MSN | 729 | 0.664 | 27.1 |
| $C_{16}$MIM-MSN | 924 | 0.950 | 30.3 |
| $C_{18}$MIM-MSN | 893 | 0.995 | 32.7 |
| $C_{14}$OCMIM-MSN | 639 | 0.695 | 26.1 |

Interestingly, a pseudo-moiré rotational pattern of mesopores was observed in the TEM micrograph of the $C_{18}$MIM-MSN material (Figure 3c), where parallel mesopores are twisted in a helical nature along the long axis of the nanorods. This pore morphology is structurally similar to a chiral mesoporous silica material recently reported by Tatsumi and co-workers.[12] In contrast to Tatsumi's material, which was synthesized in the presence of a *chiral* surfactant template, the $C_{18}$MIM-MSN material was prepared by using an *achiral* surfactant ($C_{18}$MIMBr) as the structure-directing agent. As indicated by the arrow-pointed areas in Figure 3c, each visible fringe represents the (100) interplanar spacing. The distance between two fringes is one-sixth of a pitch or a 60° rotation through the center of the long axis. It is noteworthy that all the particles shown in Figure 3c appeared to have rotations of approximately 120° regardless of particle size. The powder XRD analysis (Figure 4c) of the $C_{18}$MIM-MSN material further confirmed the twisted hexagonal ordering of the mesopores as evidenced by the diffraction pattern of an intense (100) peak along with a well-resolved (110) and a broadened (200) peak. The handedness of the rotation (right- or left-handed) could not be determined from the TEM analysis. As discussed in Tatsumi's report,[12] the ratio of the left- and right-handedness of their chiral mesoporous silica material (65/35, left/right) was not entirely governed by the intrinsic chirality of the surfactant template since only the *L*-enantiomer of the chiral surfactant was employed. In our case, we hypothesized that, as the alkyl chain lengths of the $C_n$MIMBr increases from $C_{14}$ to $C_{18}$, tighter intermolecular packing between the methylimidazolium headgroups of the achiral $C_{18}$MIMBr molecules might have occurred. Given the planar structure of the imidazolium group, such tight packing would perhaps cause a staggered wadding of the $C_{18}$MIMBr molecules and twisted the micelles into a helical structure.

This assumption was further investigated by the TEM and XRD analyses of the $C_{14}$OCMIM-MSN material that was synthesized with $C_{14}$OCMIMCl, which is a similarly sized

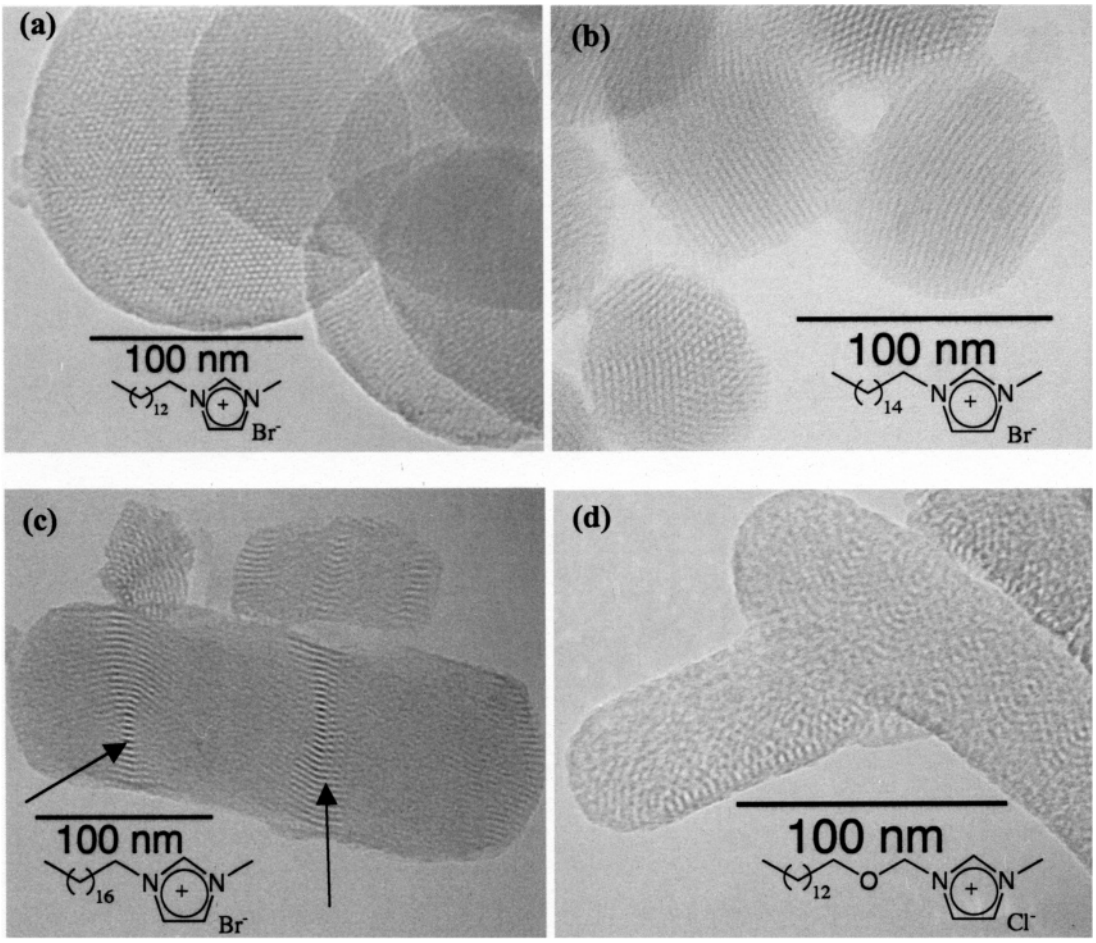


**Figure 3.** Transmission electron micrographs of $C_n$MIM-MSN materials. (a) $C_{14}$MIM-MSN, (b) $C_{16}$MIM-MSN, (c) $C_{18}$MIM-MSN, and (d) $C_{14}$OCMIM-MSN. These micrographs were obtained from a Phillips CM30 TEM operated at 300 kV.

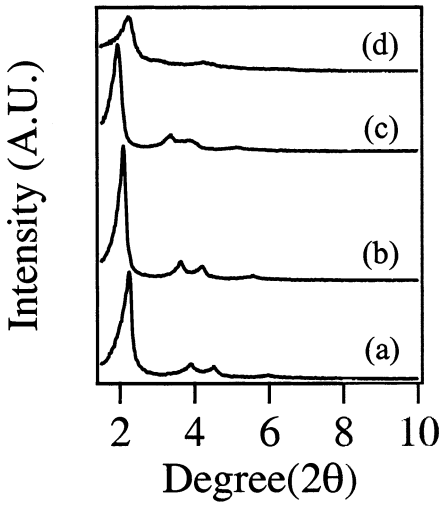


**Figure 4.** Low angle powder X-ray diffraction patterns of RTIL-removed $C_n$MIM-MSN materials. (a) $C_{14}$MIM-MSN, (b) $C_{16}$MIM-MSN, (c) $C_{18}$MIM-MSN, and (d) $C_{14}$OCMIM-MSN. The diffraction data were collected on a Scintag XRD 2000 X-ray diffractometer using Cu Kα radiation. The samples were scanned from 1.5° to 10° ($2\theta$) with a step size of 0.02° and a count time of 0.5 s at each point.

molecule in comparison with the $C_{16}$MIMBr that gave rise to a MCM-41 type mesoporous structure. The mesoporous structure of the $C_{14}$OCMIM-MSN material appeared to be disordered as indicated by a broad XRD diffraction peak at 4.22° representing superimposed (110) and (200) peaks (Figure 4d). The TEM micrograph shown in Figure 3d is also consistent with this observation. Given that the hydrophilic polar region of $C_{14}$OCMIM, with the ether moiety close to the methylimidazolium headgroup, is significantly larger of that of $C_{16}$MIM, the results support our theory that the micellar structure and packing is strongly influenced by the alkyl chain length of the alkylimidazolium template.

It is widely known that cationic surfactants possess antibacterial properties; several can be found in household soaps and detergents.[13] A recent report[11] in the literature has demonstrated the antibacterial activity of $C_{14}$OCMIMCl on both Gram (+) and Gram (−) microbes. The mechanism of the antibacterial activity of $C_{14}$OCMIMCl was attributed to the electrostatic interaction of phosphate groups on the microbial cell wall and the cationic methylimidazolium headgroup of the RTIL. Also, the organic tail region embeds itself in the lipid bilayer. This, in turn, leads to the free flow of electrolytes out of the microbe and causes the cell death. This is believed to be the mechanism of cell death for the other RTIL as well.

The antibacterial activities of the $C_{16}$MIMBr and $C_{14}$-OCMIMCl were measured by three methods: disk diffusion assay, minimal inhibitory concentration (MIC), and minimal

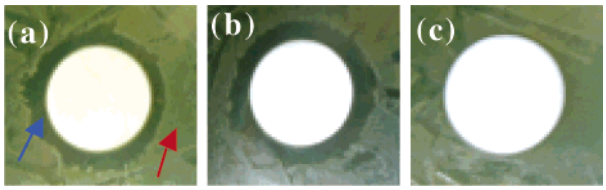


**Figure 5.** Disk diffusion assay of 15 mM $C_{16}$MIM-MSN (a), $C_{14}$-OCMIM-MSN (b), and phosphate buffer (c) on a lawn of *E. coli K12*. The red arrow points to an area of microbial lawn and the blue arrow points to the zone of clearing caused by the diffusion of RTIL.

bactericidal concentration (MBC). The disk diffusion assay was determined by placing a 25 mm cellulose disk saturated with 15 mM of $C_{16}$MIMBr and $C_{14}$OCMIMCl in 100 mM phosphate buffer (pH 7.4) onto agar plates seeded with *E. coli K12*. As depicted in Figure 5, the results of the disk diffusion assay showed an average of 35 mm of microbial clearing for $C_{16}$MIMBr and $C_{14}$OCMIMCl. The control (a cellulose disk saturated with 100 mM phosphate buffer pH 7.4) showed no antibacterial activity (Figure 5c). The MIC and MBC concentrations were determined by dissolving 10 different concentrations (10 to 100 $\mu$M) of $C_{16}$MIMBr and $C_{14}$OCMIMCl in broth media, inoculated in a 1:1 ratio with stock *E. coli K12* culture, and visually determining the lowest concentration that lacked bacteria growth for the MIC. The MBC was measured by spreading one loopful from each dilution onto the agar plates and visually determining the lowest concentration of RTIL that supported no colony formation. The MIC of both RTILs was 30 $\mu$M. The MBC of the RTILs deviated slightly from one another. The MBC of $C_{16}$MIMBr was 100 $\mu$M and the MBC of $C_{14}$OCMIMCl was 70 $\mu$M.

The antibacterial activities of $C_{16}$MIM-MSN and $C_{14}$-OCMIM-MSN were measured by series dilution for 24 h at 25 °C and 48 h at 37 °C as shown in Figure 6a and b, respectively. The two MSNs were suspended in 6 mL of tryptic soy broth with 0.6% yeast extract and inoculated with 1 mL of 18 h stock culture of *E. coli K12*. At various times, aliquots of each sample were diluted and plated on tryptic soy agar with 0.6% yeast extract. The plates were incubated for 18 h. Colonies were counted and recorded for dilutions containing between 30 and 300 colonies. In contrast to the similar MBC values for the free RTILs, $C_{16}$MIM-MSN exhibited a antibacterial activity superior to that of $C_{14}$-OCMIM-MSN by 1000-fold. The diffusion of both RTIL from the pores slowed at 25 °C. The pronounced difference in antibacterial activity between the two RTIL-MSN materials could be attributed to the different release profiles of the pore-encapsulated RTIL molecules. According to the aforementioned TEM analyses, the pore morphologies of these two samples are very different. $C_{16}$MIM-MSN has hexagonal array ordered pores that all line up parallel, while $C_{14}$-OCMIM-MSN has a disordered pore arrangement. It is plausible that the rate of RTIL release via diffusion from the parallel hexagonal channels of $C_{16}$MIM-MSN would be faster than that of the disordered pores of $C_{14}$OCMIM-MSN. In addition to pore morphology, the mass transfer of RTIL from the tubular particles ($C_{14}$OCMIM-MSN) will be considerably slower than the spherical particle ($C_{16}$MIM-MSN). The antibacterial activity of the as-synthesized, cetyltrimethylammonium bromide (CTAB) surfactant-containing MCM-41 silica prepared by the conventional methods[1] was measured by the same method and found to have similar activity as $C_{16}$MIM-MSN (see Supporting Information Figure S1). Also, we have discovered that the rates of release of RTILs from these MSN materials significantly depend on the total ionic strength of the solutions. The dependence of the release of RTIL on total ionic strength was measured by $^1$H NMR. Equal quantities (50 mg) of $C_{16}$MIM-MSN were suspended in sodium chloride solutions of various concentrations. After stirring at room temperature for 18 h, the tubes were centrifuged and the supernatants were collected. The water was evaporated under reduced pressure and the RTIL was dissolved in $CDCl_3$ (0.9 mL) with $CH_2Cl_2$ (4 $\mu$L) used as an internal standard to quantify the amount of RTIL released from the MSNs. As depicted in the Supporting Information (Figure S2), the amount of $C_{16}$MIM ($y$) released from the $C_{16}$MIM-MSN could be fitted to eq 1

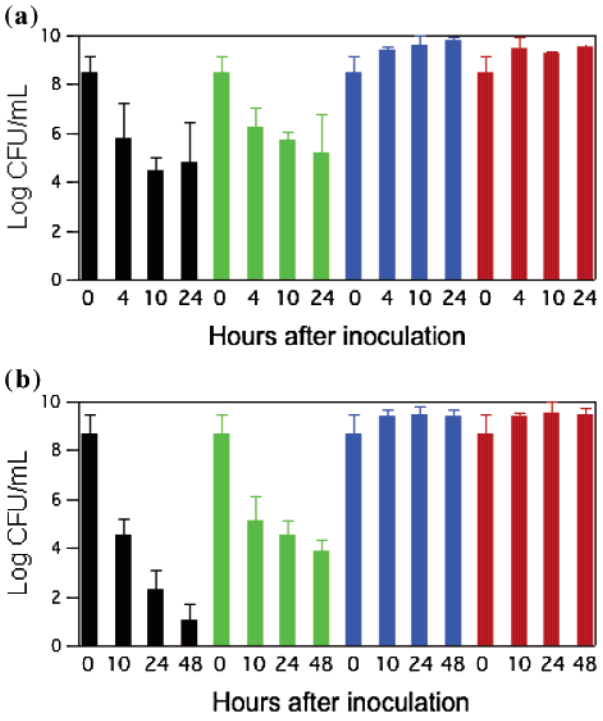


**Figure 6.** Histogram of the antibacterial activity of $C_n$MIM-MSNs against *E. coli K12* at 25 °C (a) and 37 °C (b). Four samples were measured at each temperature: $C_{16}$MIM-MSN (black bars), $C_{14}$-OCMIM-MSN (green bars), RTIL-removed $C_{16}$MIM-MSN (blue bars), and blank control (no silica material) (red bars).

$$y = -14 + 20 \cdot x^{0.05} \quad (1)$$

where $x$ is the molar concentration of the total ionic strength of the solution.

In conclusion, we have demonstrated that the particle and pore morphology of mesoporous silica nanoparticle materials could be tuned by using various room-temperature ionic liquids as synthetic templates. The antibacterial activities of two RTIL-MSNs have been measured against *E. coli K12*.

The antibacterial activity was dependent on the rate of diffusional release of the pore-encapsulated RTIL, which was governed by the particle and pore morphology of the MSN materials. By further functionalizing the surface of these RTIL-MSN materials with various organic moieties, we envision that these materials could serve as a new generation of controlled release delivery nanodevices for various applications.

**Acknowledgment.** This research was supported by NSF (CHE-0239570). The authors thank Dr. M. J. Kramer and Dr. L. S. Chumbley for experimental assistance in TEM measurements of the materials and helpful discussions.

**Supporting Information Available:** Figures describing antibacterial activity of CTAB-MSNs against *E. coli K12* and the amount of $C_{16}$MIM ($y$) released from the $C_{16}$MIM-MSN. This material is available free of charge via the Internet at http://pubs.acs.org.

## References

(1) (a) Beck, J. S.; Vartuli, J. C.; Roth, W. J.; Leonowicz, M. E.; Kresge, C. T.; Schmitt, K. D.; Chu, C. T. W.; Olson, D. H.; Sheppard, E. W. *J. Am. Chem. Soc.* **1992**, *114*, 10834−10843. (b) Kresge, C. T.; Leonowicz, M. E.; Roth, W. J.; Vartuli, J. C.; Beck, J. S. *Nature (London)* **1992**, *359*, 710−712.

(2) Zhao, D.; Feng, J.; Huo, Q.; Melosh, N.; Frederickson, G. H.; Chmelka, B. F.; Stucky, G. D. *Science* **1998**, *279*, 548−552.

(3) Bagshaw, S. A.; Prouzet, E.; Pinnavaia, T. J. *Science* **1995**, *269*, 1242−1244.

(4) Ryoo, R.; Kim, J. M.; Ko, C. H.; Shin, C. H. *J. Phys. Chem.* **1996**, *100*, 17718−17721.

(5) Inagaki, S.; Koiwai, A.; Suzuki, N.; Fukushima, Y.; Kuroda, K. *Bull. Chem. Soc. Jpn.* **1996**, *69*, 1449−1457.

(6) (a) Lin, V. S. Y.; Lai, C.-Y.; Huang, J.; Song, S.-A.; Xu, S. *J. Am. Chem. Soc.* **2001**, *123*, 11510−11511. (b) Radu, D. R.; Lai, C.-Y.; Wiench, J. W.; Pruski, M.; Lin, V. S. Y. *J. Am. Chem. Soc.* **2004**, *126*, 1640−1641. (c) Casasus, R.; Marcos, M. D.; Martinez-Manez, R.; Ros-Lis, J. V.; Soto, J.; Villaescusa, L. A.; Amoros, P.; Beltran, D.; Guillem, C.; Latorre, J. *J. Am. Chem. Soc.* **2004**, *126*, 8612−8613.

(7) (a) Huh, S.; Chen, H.-T.; Wiench, J. W.; Pruski, M.; Lin, V. S. Y. *J. Am. Chem. Soc.* **2004**, *126*, 1010−1011. (b) Lin, V. S. Y.; Radu, D. R.; Han, M.-K.; Deng, W.; Kuroki, S.; Shanks, B. H.; Pruski, M. *J. Am. Chem. Soc.* **2002**, *124*, 9040−9041. (c) Corma, A. *Chem. Rev.* **1997**, *97*, 2373−2419 and references therein. (d) Thomas, J. M. *J. Mol. Catal. A* **1999**, *146*, 77−85. (e) Brunel, D.; Blanc, A. C.; Galarneau, A.; Fajula, F. *Catal. Today* **2002**, *73*, 139−152.

(8) (a) Lai, C.-Y.; Trewyn, B. G.; Jeftinija, D. M.; Jeftinija, K.; Xu, S.; Jeftinija, S.; Lin, V. S. Y. *J. Am. Chem. Soc.* **2003**, *125*, 4451−4459. (b) Mal, N. K.; Fujiwara, M.; Tanaka, Y.; Taguchi, T.; Matsukata, M. *Chem. Mater.* **2003**, *15*, 3385−3394. (c) Vallet-Regi, M.; Ramila, A.; del Real, R. P.; Perez-Pariente, J. *Chem. Mater.* **2001**, *13*, 308−311. (d) Tourne-Peteilh, C.; Brunel, D.; Begu, S.; Chiche, B.; Fajula, F.; Lerner, D. A.; Devoisselle, J.-M. *New J. Chem.* **2003**, *27*, 1415−1418.

(9) (a) Huh, S.; Wiench, J. W.; Yoo, J.-C.; Pruski, M.; Lin, V. S. Y. *Chem. Mater.* **2003**, *15*, 4247−4256. (b) Huh, S.; Wiench, J. W.; Trewyn, B. G.; Song, S.; Pruski, M.; Lin, V. S. Y. *Chem. Commun.* **2003**, 2364−2365.

(10) (a) Zhou, Y.; Antonietti, M. *Adv. Mater.* **2003**, *15*, 1452−1455. (b) Zhou, Y.; Schattka, J. H.; Antonietti, M. *Nano Lett.* **2004**, *4*, 477−481. (c) Zhou, Y.; Antonietti, M. *Chem. Mater.* **2004**, *16*, 544−550. (d) Lee, B.; Luo, H.; Yuan, C. Y.; Lin, J. S.; Dai, S. *Chem. Commun.* **2004**, 240−241.

(11) Pernak, J.; Sobaszkiewicz, K.; Mirska, I. *Green Chem.* **2003**, *5*, 52−56.

(12) Che, S.; Liu, Z.; Ohsuna, T.; Sakamoto, K.; Terasaki, O.; Tatsumi, T. *Nature* **2004**, *429*, 281−284.

(13) Davis, B.; Jordan, P. An Overview of the Biocidal Activity of Cationics and Ampholities. In *Industrial Applied Surfactants II*; Karsa, D. R., Ed.; Royal Society of Chemistry: Cambridge, 1990; Vol. 77, pp 195−210.

NL048774R